

# Slow and fast particles in shear-driven jamming: critical behavior and finite size scaling

Peter Olsson

*Department of Physics, Umeå University, 901 87 Umeå, Sweden*

(Dated: June 14, 2023)

We do shear-driven simulations of a simple model of non-Brownian particles in two dimensions. By examining the velocity distribution at different densities and shear rates we find strong evidence for the existence of two different processes, respectively dominated by the slower and the faster particles—the slow process and the fast process. The leading divergence in the shear viscosity is governed by the fast process. An examination of height and position of the low-velocity peak in the distribution demonstrates that it is the slow process that is responsible for the correction-to-scaling term in the critical scaling analysis. We further find that the presence of velocity correlations across large distances is primarily due to the slow process which implies that the diverging viscosity and the diverging correlation length are only indirectly related.

PACS numbers: 63.50.Lm, 45.70.-n 83.10.Rs

Particle transport is ubiquitous in both industry and every-day life with varying behaviors due e.g. to differing particle properties and geometries. A reasonable approach in the quest for a better understanding of the slowing down of the dynamics, e.g. because of an increase in density, is to first examine simplified models. One of the simplest possible consists of a collection of circular disks in two dimensions with contact-only interactions [1]. When such a collection of particles is driven at a constant shear strain rate  $\dot{\gamma}$  [2], the system develops a shear stress  $\sigma$ , and the shear viscosity,  $\eta \equiv \sigma/\dot{\gamma}$ , diverges as the jamming density,  $\phi_J$ , is approached from below. For the conceptually simple case of hard disks and overdamped dynamics this is seen in an algebraic divergence,  $\eta \sim (\phi_J - \phi)^{-\beta}$ . This divergence is related to the increase in contact number  $z$  towards the isostatic value,  $z_c - z \sim (\phi_J - \phi)^{u_z}$ . In the thermodynamic limit the isostatic contact number is  $z_c = 2d$  [3]; see Ref. [4] for the generalization to finite  $N$ . In terms of the contact number deficit the divergence becomes  $\eta \sim (z_c - z)^{-\beta/u_z}$ .

A hallmark of critical phenomena is a diverging spatial correlation length. It has also long been realized that particle motion in sheared systems becomes increasingly collective as the jamming density is approached [5–8]. In a recent analysis of the velocity field [9] it was further found that fluctuations in the rotation and the divergence of the velocity field behave differently, and that the length related to the rotations appears to be the more important one, diverging as  $\xi \sim (\phi_J - \phi)^{-\nu}$ , with  $\nu \approx 1$  [9].

Because of difficulties with numerically simulating the dynamics of hard particles, simulations are commonly performed with elastic particles with forces related to the particle overlaps. The shear viscosity has then a strong shear strain rate dependence—see Fig. 1(a)—and in attempted critical scaling analyses [10, 11] it has furthermore become clear that one also needs to include a correction-to-scaling term [11, 12]. In two dimensions (2D) such determinations of  $\beta$  have typically given val-

ues in the range  $\beta = 2.2$  through  $2.83$  [11–13]. For the combination  $\beta/u_z$  different methods that directly probe the hard disk limit give  $\beta/u_z = 1/0.38 = 2.63$  [14] and  $\beta/u_z = 2.69$  [15]. (Determinations in three dimensions tend to give higher values,  $\beta/u_z \approx 3.3$  [16] or  $\beta/u_z = 3.7 \pm 0.7$  [17]. An attempt to explain this dependence on dimensionality in terms of a finite size effect is discussed in [18, 19].)

From analytical considerations the exponent has however been argued to be  $\beta/u_z \approx 3.41$  [16, 20] and it has then been claimed that the determinations quoted above for 2D are incorrect due to the neglect of logarithmic corrections to scaling [16, 18, 20]. Though this explanation is a possibility, it could also be that the discrepancy only points to a lack of understanding of the phenomenon of shear-driven jamming.

In the present Letter we present evidence for a novel picture that describes shear-driven jamming as being controlled by two different processes dominated by the slow and the fast particles, respectively, and accordingly coined the “slow process” and the “fast process”. The fast process is responsible for the leading term in the divergence of the shear viscosity and is dominated by particles in the tail of the velocity distribution [21]. The slow process leads to the correction-to-scaling term [11, 12], and arises from particles at and below the low-velocity peak in the distribution. It is further found that the presence of velocity correlations across large distances is related to the slow process whereas the fast process appears to be short range correlated, only. The present Letter gives a short description of a comprehensive examination of shear-driven jamming; a more detailed discussion is given in Ref. [22], except for the finite size dependence, which will be discussed elsewhere [23]. The analyses presented here work the same also in three and four dimensions, presentations of these results will however also be deferred to a later publication.

We simulate a bidisperse collection of particles in 2D

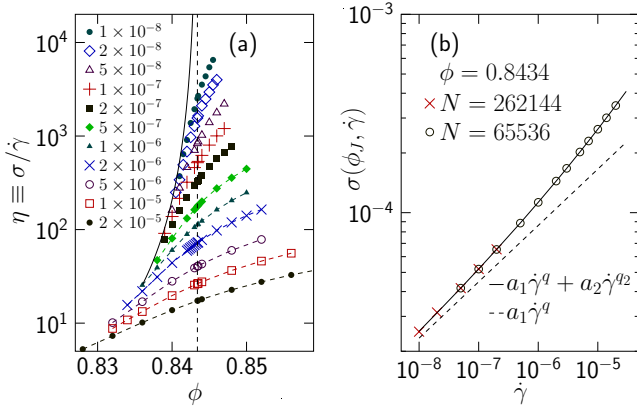


FIG. 1. The divergence of the shear viscosity. Panel (a) is the shear viscosity  $\eta \equiv \sigma/\dot{\gamma}$  for different shear strain rates. The vertical dashed line is  $\phi_J$  and the solid line is the approximate critical divergence  $\eta(\phi, \dot{\gamma} \rightarrow 0) \sim (\phi_J - \phi)^{-\beta}$ ,  $\beta = 2.7$ . Panel (b) which is  $\sigma$  vs  $\dot{\gamma}$  at  $\phi = 0.8434 \approx \phi_J$  illustrates the determination of the exponents  $q$  and  $q_2$  defined in Eq. (3).

with equal number of particles of two different sizes. The total number of particles is  $N = 65536$  particles, if not otherwise noted. The small particles have diameter  $d_s = 1$  and the size ratio is 1.4 [1]. For particles in contact we define the relative overlap  $\delta_{ij} = 1 - r_{ij}/d_{ij}$  where  $r_{ij}$  is the distance between particles  $i$  and  $j$  and  $d_{ij}$  is the sum of their radii. The contact interaction is from the potential energy  $V_p(r_{ij}) = \epsilon \delta_{ij}^2/2$ ; we take  $\epsilon = 1$ . The force on particle  $i$  from particle  $j$  is  $\mathbf{f}_{ij}^{\text{el}} = -\nabla_i V_p(r_{ij})$ , which gives  $f_{ij}^{\text{el}} = \epsilon \delta_{ij}/d_{ij}$ . We do shearing simulations with a time-dependent shear strain  $\gamma = \dot{\gamma}t$  and Lees-Edwards boundary conditions [24] on a system with volume  $V = L \times L$ . The shearing gives an average homogenous velocity profile  $= \dot{\gamma}y\hat{x}$  but our focus will be on the non-affine velocity, which is the particle velocity relative to this velocity profile,  $\mathbf{v}_i = \mathbf{v}_i^{\text{tot}} - \dot{\gamma}y_i\hat{x}$ . Related to the non-affine velocity is the dissipative force  $\mathbf{f}_i^{\text{dis}} = -k_d\mathbf{v}_i$ . We simulate with overdamped dynamics such that  $\mathbf{f}_i^{\text{el}} + \mathbf{f}_i^{\text{dis}} = 0$  which becomes  $\mathbf{v}_i = \mathbf{f}_i^{\text{el}}/k_d$ . We take  $k_d = 1$  and the unit of time  $\tau_0 = d_s^2 k_d / \epsilon = 1$ . The shear stress is  $\sigma = -\langle \mathbf{p}_{xy} \rangle$  from the pressure tensor which is obtained from the forces between the contacting particles,  $\mathbf{p}^{\text{el}} = V^{-1} \sum_{i < j} \mathbf{f}_{ij}^{\text{el}} \otimes \mathbf{r}_{ij}$ . Because of the large  $N$  in our simulations the fluctuations in pressure  $\equiv \frac{1}{2}(\mathbf{p}_{xx}^{\text{el}} + \mathbf{p}_{yy}^{\text{el}})$  during the run are very small.

The analyses below will be done in terms of the shear stress  $\sigma$  but to illustrate the jamming transition Fig. 1(a) shows  $\eta(\phi, \dot{\gamma}) \equiv \sigma(\phi, \dot{\gamma})/\dot{\gamma}$  for shear strain rates  $\dot{\gamma} = 10^{-8}$  through  $2 \times 10^{-5}$ . The transition is shown by the rapid increase of  $\eta$  with  $\phi$ , which in the  $\dot{\gamma} \rightarrow 0$  limit approaches  $\eta \sim (\phi_J - \phi)^{-\beta}$ , with  $\beta \approx 2.7$ , illustrated by the solid line. The analyses of this kind of data (and the similar  $\eta_p = p/\dot{\gamma}$ ) in the literature [10, 11] rely on the standard

scaling assumption [25],

$$\sigma(\phi, \dot{\gamma}) b^{y/\nu} = \bar{g}_\sigma(\delta\phi b^{1/\nu}, \dot{\gamma} b^z) + b^{-\omega} \bar{h}_\sigma(\delta\phi b^{1/\nu}, \dot{\gamma} b^z). \quad (1)$$

Here  $b$  is a length rescaling factor,  $y$  is the scaling dimension of  $\sigma$ ,  $\nu$  is the correlation length exponent,  $\delta\phi = \phi - \phi_J$ ,  $z$  is the dynamical exponent,  $\omega$  is the correction-to-scaling exponent and  $\bar{g}_\sigma$  and  $\bar{h}_\sigma$  are unknown scaling functions. With  $b = \dot{\gamma}^{-1/z}$  in Eq. (1) together with  $q = y/z\nu$  and  $q_2 = q + \omega/z$  one finds

$$\sigma(\phi, \dot{\gamma}) = \dot{\gamma}^q g_\sigma\left(\frac{\phi - \phi_J}{\dot{\gamma}^{1/z\nu}}\right) + \dot{\gamma}^{q_2} h_\sigma\left(\frac{\phi - \phi_J}{\dot{\gamma}^{1/z\nu}}\right). \quad (2)$$

In the fitting of Ref. [11] the scaling functions were taken to be exponentials of polynomials in  $(\phi - \phi_J)/\dot{\gamma}^{1/z\nu}$ , and the parameters of these polynomials together with  $\phi_J$  and the critical exponents were adjusted to get the best possible fit. [Since  $\omega > 0$ , as it is an irrelevant scaling variable, it follows that  $q_2 > q$ , and that for  $\eta$  the two terms of Eq. (2) scale as  $\dot{\gamma}^{q-1}$  and  $\dot{\gamma}^{q_2-1}$ , which implies that the first term is the more divergent one as  $\dot{\gamma} \rightarrow 0$ .]

As shown in Eq. (2) the scaling expression for  $\sigma(\phi, \dot{\gamma})$  consists of two different terms, as first reported in Ref. [11], and the question that we set out to answer in the present Letter is the physical mechanisms behind these two terms. To simplify the analyses we here focus on the behavior at the jamming density  $\phi = \phi_J$ . An alternative, which is to examine the simulations in the hard disk limit, is shown in Sec. III E of Ref. [22]. At  $\phi = \phi_J$  Eq. (2) simplifies to,

$$\sigma(\phi_J, \dot{\gamma}) = a_1 \dot{\gamma}^q + a_2 \dot{\gamma}^{q_2}. \quad (3)$$

With  $\phi_J \approx 0.8434$  [11, 26] and with the methods described in Ref. [22] we obtain the exponents  $q = 0.284(2)$  and  $q_2 = 0.567(7)$ , in good agreement with previous works [11]. The prefactors are  $a_1 = 0.00437$  and  $a_2 = 0.067$ . The fit is shown in Fig. 1(b).

To examine the shear stress in a novel way we turn to the properties of the velocity distribution  $\mathcal{P}(v)$  calculated from the non-affine velocities  $v_i \equiv |\mathbf{v}_i|$ , normalized such that  $\int \mathcal{P}(v) dv = 1$ . Fig. 2(a) shows  $\mathcal{P}(v)$  vs  $v$  at  $\phi = 0.8434 \approx \phi_J$  for  $\dot{\gamma} = 10^{-8}$  through  $2 \times 10^{-5}$ . For each shear strain rate there is a peak at  $v = v_p$  with peak height  $\mathcal{P}_p = \mathcal{P}(v_p)$ . A key observation is now that the data up to and slightly above the peak collapse to a common function, as shown in Fig. 2(b), when  $\mathcal{P}(v)$  and  $v$  are rescaled to make the peaks fall on top of each other. The same is true also for  $\mathcal{P}(v)$  from a range of densities both below and above  $\phi_J$  (see [22]). At higher velocities  $\mathcal{P}(v)$  is algebraic,  $\mathcal{P}(v) \sim v^{-r}$ , with an exponent  $r$  that varies with  $\phi$  and  $\dot{\gamma}$ . [Earlier analyses suggest that  $r \rightarrow 3$  as jamming is approached [21]. The distributions are eventually cut off exponentially at large  $v$ .]

We now set out to show that the second term in Eq. (3) is related to the peak in  $\mathcal{P}(v)$ . With the well known power

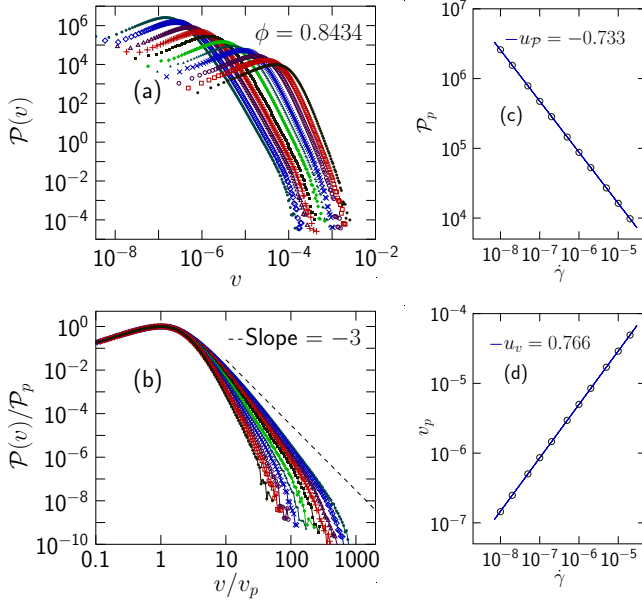


FIG. 2. Velocity distributions at  $\phi = 0.8434 \approx \phi_J$ . Panel (a) gives  $\mathcal{P}(v)$  for several different shear strain rates with symbols as in Fig. 1(a). Each data set has a clear peak and panel (b) shows the same data rescaled to make the peaks coincide. It is then found that the rescaled  $\mathcal{P}(v)$  collapse below and up to the peak whereas the data above the peak depend strongly on  $\dot{\gamma}$ . At high velocities the distributions decay algebraically with a  $\dot{\gamma}$ -dependent exponent. Panels (c) and (d) show the algebraic dependences of peak height and position on  $\dot{\gamma}$ :  $\mathcal{P}_p \sim \dot{\gamma}^{u_P}$  and  $v_p \sim \dot{\gamma}^{u_v}$ .

balance  $\sigma\dot{\gamma} = (N/V)k_d \langle v^2 \rangle$ , which is a relation between input power  $V\sigma\dot{\gamma}$  and dissipated power  $Nk_d \langle v^2 \rangle$  [27], the shear stress may be written in terms of  $\mathcal{P}(v)$  as

$$\sigma = \frac{N}{V} \frac{k_d}{\dot{\gamma}} \int \mathcal{P}(v) v^2 dv. \quad (4)$$

Introducing  $x = v/v_p$  and  $f(x) = \mathcal{P}(v)/\mathcal{P}_p$ , the contribution to  $\sigma$  from velocities up to the peak becomes

$$S(v_p) = \frac{N}{V} k_d W_p \int_0^1 f(x) x^2 dx, \quad (5)$$

where  $W_p = \mathcal{P}_p v_p^3 / \dot{\gamma}$ . Fig. 2(c) and (d) show that peak height and position depend algebraically on  $\dot{\gamma}$ :  $\mathcal{P}_p \sim \dot{\gamma}^{u_P}$ , with  $u_P = -0.733$ , and  $v_p \sim \dot{\gamma}^{u_v}$ , with  $u_v = 0.766$ . For the  $\dot{\gamma}$ -dependence of  $S(v_p) \sim W_p$  we then find

$$W_p(\phi_J, \dot{\gamma}) \sim \dot{\gamma}^{u_P + 3u_v - 1} \sim \dot{\gamma}^{u_w}, \quad (6)$$

with  $u_w = 0.565$ , and note that this is in excellent agreement with  $q_2 \approx 0.567$  from the fit of  $\sigma(\phi, \dot{\gamma})$  to Eq. (3).

We now turn to the magnitude of the contribution due to the slow process. We formally split  $\mathcal{P}(v)$  into two parts for the slow and the fast processes,  $\mathcal{P}(v) = \mathcal{P}_s(v) + \mathcal{P}_f(v)$ . With this splitting the dissipation from the slow process

becomes  $\mathcal{D}_s = k_d \int \mathcal{P}_s(v) v^2 dv$ . We get  $\sigma_s = (N/V\dot{\gamma})\mathcal{D}_s$ , which means that  $\sigma_s$  is determined from the dissipation.

To demonstrate that  $\sigma_s$  from the dissipation is indeed equal to the correction-to-scaling term  $a_2 \dot{\gamma}^{q_2}$ , in Eq. (3), we use the reasoning behind Eq. (5) with  $f_s(x) \equiv \mathcal{P}_s(v)/\mathcal{P}_p$ , to get

$$\sigma_s = \frac{N}{V} k_d W_p I_2, \quad (7)$$

where  $I_2 \equiv \int_0^\infty f_s(x) x^2 dx$ . We find that the choice  $I_2 = 3.4$  gives a good agreement at  $\phi_J$  between  $\sigma_s$  and the second term of Eq. (3). In Ref. [22] it is shown that it is possible to construct a reasonable  $f_s(x)$  that is equal to  $f(x)$  below the peak, decays exponentially at larger  $v$ , and gives  $I_2 = 3.4$ . This shows that not only the  $\dot{\gamma}$ -dependence, but also the magnitude, of the correction-to-scaling term is consistent with it being due to the rescaled  $f_s(x)$ .

In Sec. III E of Ref. [22] we show this kind of analysis for data from the hard disk limit at  $\phi < \phi_J$  and show that it works well and gives consistent results with the results here, through analyses from different  $\dot{\gamma}$  at  $\phi_J$ .

We now turn to analyzing the velocity correlations and then first note that the very wide distribution of particle velocities is due to the fact that the particle velocity is  $v_i = f_i/k_d$ , where the net force  $f_i \equiv \sum_j f_{ij}$  is usually much smaller than the typical contact force,  $f_{ij}$ , since the contact forces usually almost balance each other out. In cases where the contact forces fail to balance each other out, as e.g. in Fig. 3(a) where the dark gray particle is squeezed between the two contacting light gray particles, this may give an unusually large net force and thereby a high velocity. The fastest particles are the ones with only two contacting particles but in the Supplemental Material we show that they nevertheless give only about 7% of the total dissipation and that most of the dissipation is due to (short) chains of fast particles. We also argue that the same mechanism that gives the fast particle in Fig. 3(a) also gives these short chains of fast particles.

In Ref. [28] it was found that the theoretically expected force distribution was obtained if contacts that were related to localized configurations were not included in the calculation, and it was further argued that these contacts were due to buckler configurations. We note the similarity of Fig. 3(a) and the buckler configuration shown in Ref. [28] and remark that particles that are irrelevant in the approach of Ref. [28] are here found to be significant. Fig. 3(a) also suggests a possible relation between some of the fast particles and irreversible contact changes in quasistatic shearing [29, 30].

It is well known [5–7] that the dynamics becomes increasingly collective as jamming is approached and a recent paper has revealed a rich behavior of the velocity correlations [9]. A large correlation length is what one would expect when particles behave as a slowly moving

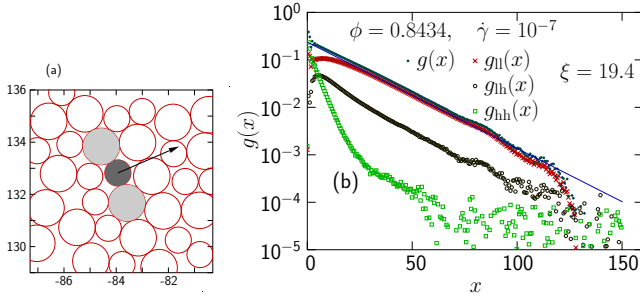


FIG. 3. Behaviors of fast particles. Panel (a) which is a snapshot at  $\phi = 0.800$  shows a particle with velocity  $v/\langle v \rangle \approx 8.5$  which has a high velocity because it is not in a force-balanced state but is squeezed between two other particles, shown by light gray. Panel (b) shows the splitting of the velocity correlation function according to the low or high velocity of the colliding particles:  $g_{ll}$  for two low velocity particles,  $g_{hh}$  for two high velocity particles, and  $g_{lh}$  due to one particle with low and one with high velocity. The key message is that the contribution to the total  $g(x)$  from two high velocity particles is very small.

fluid, but it is less clear what to expect for high velocity particles, as in Fig. 3(a), which move erratically because of squeezing. To answer this question Fig. 3(b) shows the velocity correlation  $g(x) = [\langle v_{\nearrow}(0)v_{\searrow}(x\hat{x}) \rangle + \langle v_{\searrow}(0)v_{\nearrow}(x\hat{x}) \rangle]/(\mathbf{v}^2/2)$  which is a measure of the rotation of the non-affine velocity field [9]. We show both  $g(x)$  from all particles and the contributions to  $g(x)$  from different sets of particles. We identify the velocities as “low” or “high” according to the threshold velocity  $v_{50}$ , chosen such that 50% of the dissipation is due to particles with  $v < v_{50}$ . This is similar to the splitting into slow and fast processes, but also different since  $\mathcal{P}_s(v)$  and  $\mathcal{P}_f(v)$  are overlapping, with no sharp threshold velocity. Fig. 3(b) shows that the full  $g(x)$  at  $\phi = 0.8434$  and  $\dot{\gamma} = 10^{-7}$  decays exponentially with a length  $\xi \approx 19.4$  and that it is the low velocity particles that strongly dominate the large distance correlation;  $g_{hh}(x)$  from two high velocity particles, contributes less than 1% to the total  $g(x)$ , for large  $x$ . We believe that this non-zero value of  $g_{hh}(x)$  is because the fast particles also get a contribution to their velocities from the slow process since they are embedded in a set of particles that behaves as a slowly moving fluid.

This therefore suggests that the large correlation length is due to the slow process, only, and this is a finding with profound consequences as it suggests that one process is responsible for the correlations whereas another process is behind the leading divergence in the viscosity, which is at odds with usual critical phenomena. The link between viscosity and correlation length would therefore seem to be an indirect one, only, and it appears that there exists some, as yet unknown, mechanism that connects the slow and the fast processes together.

The lack of large distance correlations of the fast particles has consequences also for the finite size dependence,

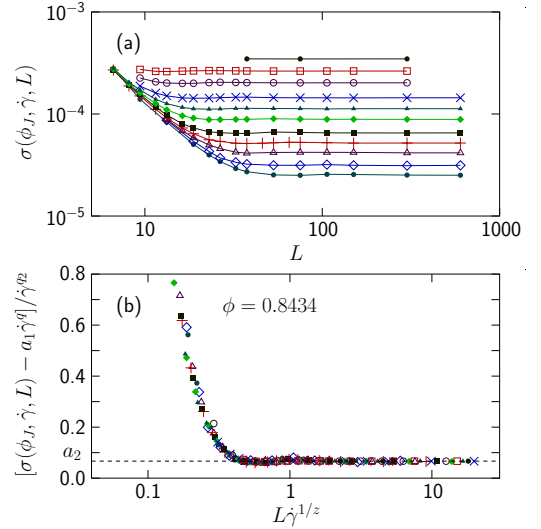


FIG. 4. Finite size scaling at  $\phi_J \approx 0.8434$ . Panel (a) is the raw data  $\sigma(\phi_J, \dot{\gamma}, L)$  for  $\dot{\gamma} = 10^{-8}$  through  $2 \times 10^{-5}$ , with symbols as in Fig. 1(a), for  $N = 32$  through 262144. Panel (b) shows that  $[\sigma - a_1 \dot{\gamma}^q]/\dot{\gamma}^{q_2}$  collapses when plotted vs  $L\dot{\gamma}^{1/z}$ , in agreement with Eq. (9). We here use  $1/z = 0.26$ , assuming  $1/z\nu = 0.26$  [11] and  $\nu = 1$  [9].

examined in simulations with different  $N \propto L^2$ . To include the  $L$ -dependence in the critical scaling analysis one adds  $b/L$  as an additional argument to the scaling functions of Eq. (1), and Eq. (3) then becomes

$$\sigma(\phi_J, \dot{\gamma}, L) = \dot{\gamma}^q \tilde{g}_\sigma(L\dot{\gamma}^{1/z}) + \dot{\gamma}^{q_2} \tilde{h}_\sigma(L\dot{\gamma}^{1/z}). \quad (8)$$

This means that one would expect  $\sigma(\phi_J, \dot{\gamma}, L)$  to be the sum of two  $L$ -dependent functions, respectively approaching  $a_1$  and  $a_2$  for large  $L$ , with different prefactors,  $\dot{\gamma}^q$  and  $\dot{\gamma}^{q_2}$ . It does however turn out that the data, shown in Fig. 4(a), fit very well to a simpler expression without any finite size dependence in the first term,

$$\sigma(\phi_J, \dot{\gamma}, L) = a_1 \dot{\gamma}^q + \dot{\gamma}^{q_2} \tilde{h}_\sigma(L\dot{\gamma}^{1/z}). \quad (9)$$

This is demonstrated in Fig. 4(b) which shows that  $[\sigma(\phi_J, \dot{\gamma}, L) - a_1 \dot{\gamma}^q]/\dot{\gamma}^{q_2}$ , with  $q$ ,  $q_2$ , and  $a_1$  the same as in Eq. (3), collapses onto a single function when plotted vs  $L\dot{\gamma}^{1/z}$ . Even though there is nothing in the formalism that excludes the possibility that the function  $\tilde{g}_\sigma(L\dot{\gamma}^{1/z})$  could be a constant  $= a_1$ , the absence of a clear finite size dependence for the leading diverging term is clearly at odds with the ordinary behavior in critical phenomena. It is however entirely in accordance with the absence of correlations across large distances in Fig. 3(b) for the particles with higher velocities, which are the ones that dominate the  $\dot{\gamma}^q$ -term.

To summarize, we provide strong evidence that shear-driven jamming is governed by two processes with different properties: The fast process is responsible for the leading divergence of the shear viscosity whereas the

slow process is behind the diverging correlation length. The absence of a direct coupling between these diverging quantities suggests that shear-driven jamming is an unusual kind of critical phenomenon.

I thank S. Teitel for many discussions and suggestions on the manuscript. The computations were enabled by resources provided by the Swedish National Infrastructure for Computing (SNIC) at High Performance Computer Center North, partially funded by the Swedish Research Council through grant agreement no. 2018-05973.

- 
- [1] C. S. O'Hern, L. E. Silbert, A. J. Liu, and S. R. Nagel, Phys. Rev. E **68**, 011306 (2003).
  - [2] D. J. Durian, Phys. Rev. Lett. **75**, 4780 (1995).
  - [3] S. Alexander, Physics Reports **296**, 65 (1998).
  - [4] C. P. Goodrich, A. J. Liu, and S. R. Nagel, Phys. Rev. Lett. **109**, 095704 (2012).
  - [5] O. Pouliquen, Phys. Rev. Lett. **93**, 248001 (2004).
  - [6] F. Lechenault, O. Dauchot, G. Biroli, and J. P. Bouchaud, Europhys. Lett. **83**, 46003 (2008).
  - [7] C. Heussinger, L. Berthier, and J.-L. Barrat, Europhys. Lett. **90**, 20005 (2010).
  - [8] D. Hexner, A. J. Liu, and S. R. Nagel, Phys. Rev. Lett. **121**, 115501 (2018).
  - [9] P. Olsson and S. Teitel, Phys. Rev. E **102**, 042906 (2020).
  - [10] P. Olsson and S. Teitel, Phys. Rev. Lett. **99**, 178001 (2007).
  - [11] P. Olsson and S. Teitel, Phys. Rev. E **83**, 030302(R) (2011).
  - [12] T. Kawasaki, D. Coslovich, A. Ikeda, and L. Berthier, Phys. Rev. E **91**, 012203 (2015).
  - [13] B. Andreotti, J.-L. Barrat, and C. Heussinger, Phys. Rev. Lett. **109**, 105901 (2012).
  - [14] E. Lerner, G. Düring, and M. Wyart, PNAS **109**, 4798 (2012).
  - [15] P. Olsson, Phys. Rev. E **91**, 062209 (2015).
  - [16] E. DeGiuli, G. Düring, E. Lerner, and M. Wyart, Phys. Rev. E **91**, 062206 (2015).
  - [17] P. Olsson, Phys. Rev. Lett. **122**, 108003 (2019).
  - [18] Y. Nishikawa, A. Ikeda, and L. Berthier, J. Stat. Phys. **182**, 37 (2021).
  - [19] P. Olsson, Phys. Rev. E **105**, 034902 (2022).
  - [20] H. Ikeda, J. Chem. Phys. **153**, 126102 (2020).
  - [21] P. Olsson, Phys. Rev. E **93**, 042614 (2016).
  - [22] (2022), see the jointly published paper in Physical Review E, P. Olsson.
  - [23] P. Olsson, "Slow and fast particles in shear-driven jamming: finite size scaling," (2022), unpublished.
  - [24] D. J. Evans and G. P. Morriss, *Statistical Mechanics of Nonequilibrium Liquids* (Academic Press, London, 1990).
  - [25] D. Vågberg, P. Olsson, and S. Teitel, Phys. Rev. E **93**, 052902 (2016).
  - [26] C. Heussinger and J.-L. Barrat, Phys. Rev. Lett. **102**, 218303 (2009).
  - [27] I. K. Ono, S. Tewari, S. A. Langer, and A. J. Liu, Phys. Rev. E **67**, 061503 (2003).
  - [28] P. Charbonneau, E. I. Corwin, G. Parisi, and F. Zamponi, Phys. Rev. Lett. **114**, 125504 (2015).
  - [29] P. Morse, S. Wijtmans, M. van Deen, M. van Hecke, and M. L. Manning, Phys. Rev. Res. **2**, 023179 (2020).
  - [30] P. J. Tuckman, K. VanderWerf, Y. Yuan, S. Zhang, J. Zhang, M. D. Shattuck, and C. S. O'Hern, Soft Matter **16**, 9443 (2020).